Solid Electrolytes Based on Lithium-containing Lanthanum Metaniobates and Metatantalates with Defect-Perovskite Structure

A. Belous*, E. Pashkova, O. Gavrilenko, O. V'yunov and L. Kovalenko
V.I. Vernadskii Institute of General & Inorganic Chemistry, Kyiv, Ukraine
*Corresp. author: Prof. A. Belous, e-mail: belous@ionc.kar.net

Abstract. The structure and transport properties of lithium-containing lanthanum metaniobates and metatantalates with defect-perovskite structure, $La_{2/3-x}Li_{3x}\square_{4/3-2x}Nb[Ta]_2O_6$, have been studied. It has been shown that the materials under investigation possess a high lithium ion-conductivity

1. Introduction

The search for solid electrolytes with high lithium ion-conductivity is very topical. In this aspect, the complex oxides $La_{2/3-x}Li_{3x}\square_{4/3-2x}Nb_2O_6$ (**I**) and $La_{2/3-x}Li_{3x}\square_{4/3-2x}Ta_2O_6$ (**II**), prepared by substituting La^{3+} for Li^+ ions in isostructural metaniobate $La_{2/3}\square_{4/3}Nb_2O_6$ (**III**) and metatantalate $La_{2/3}\square_{4/3}Ta_2O_6$ (**IV**) with defect-perovskite structure, respectively, may be promising (Fig. 1) [1]. The crystal structure of these compounds are derivatives of perovskite structure. References [2–5] show that the filling of every other layer in the perovskite lattice with the structural unit 2/3 La^{3+} + 1/3 ❑ (❑-vacancies) is statistical character. The doubling of the parameter *c* is associated with the alternation of the above empty layers (sites 1c) and layers filled with La^{3+} atoms two-thirds full (sites 1a). The La^{3+} atoms are in cuboctahedra, and the Nb or Ta atom in octahedral. The Nb–O (Ta–O) distances differ from those in ideal perovskite, which is due to the displacement of Nb and Ta atoms along the *Z* axis towards empty layers. The difference of the structure **I** from the structure **II** is that the vectors of displacement of the oxygen atoms that lie on the unit cell faces O_3 and O_4 in the opposite direction to the displacement of Nb[Ta] atoms are not the same, leading to rhombic distortion of the Nb and La polyhedra (space group of **III** is Pmmm, space group of **IV** is P4/mmm). The presence of channels and a sufficient number of vacancies in the basic structures **III** and **IV** creates pre-requisites for the occurrence of lithium ion-conduction in lithium-containing lanthanum metaniobates and metatantalates.

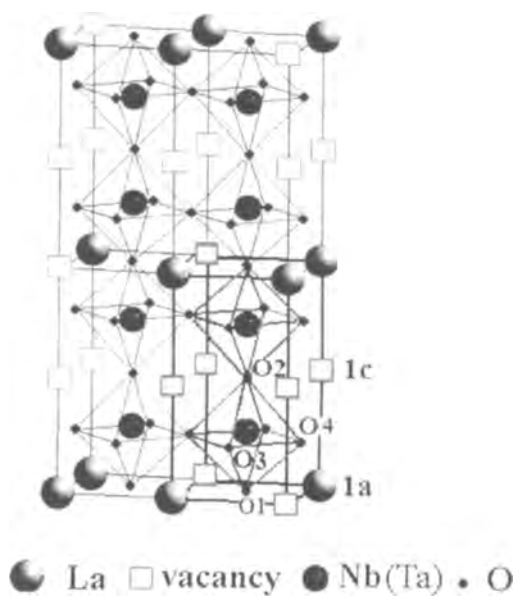

Fig. 1. Structure of defect perovskite $La_{2/3}\square_{4/3}Nb_2O_6$. Positions of atoms: La (1a) 0 0 0; Nb (2t) 1/2 1/2 z; O_1 (1f) 1/2 1/2 0; O_2 (1h) 1/2 1/2 1/2; O_3 (2s) 1/2 0 z; O_4 (2r) 0 1/2 z. Position of vacancies (1c) 0 0 1/2. Positions 2s and 2r degenerate to 4i for $La_{2/3}\square_{4/3}Ta_2O_6$.

The aim of the present work was to study crystallographic features and transport properties of lithium-containing lanthanum metaniobates and metatantalates corresponding to the formulas **I** and **II** at x = 0 – 0.62.

2. Experimental Description

Solid solutions of the systems **I** and **II** were synthesized using solid-state reactions technique. Extra pure Li_2CO_3,

Nb_2O_5 and La_2O_3 of the sort "LO-1" were used as starting reagents. To remove moisture and adsorbed gases, heat treatments of the reagents were made for 2 h at 570 K (Li_2CO_3), 1020 K (Nb_2O_5) and 1220 K (La_2O_3). Taking into account the high hygroscopicity of the starting components and the ability of La_2O_3 to actively absorb CO_2 from air, the reagents were weighed just after heat treatment. Homogenizing grinding was performed in a vibrating mill in acetone for 5 h. The blend was evaporated, dried additionally at 370 K (1 h), and sieved through a nylon net (0.063 mm). Powders were pressed into tablets (d = 10 mm) under a pressure of 0.5 MPa/cm^2 and synthesized at 1320 K (2 h) in a furnace with heaters made of silicon carbide. Samples had been ground, homogenized in a vibrating mill and dried. A 5% aqueous solution of polyvinyl alcohol was added as plasticizer. The pressed metaniobate and metatantalate samples were sintered at 1400–1520 K (1 h) and 1700–1770 K (1 h), respectively.

The phases were identified by X-ray powder diffractograms (XRPD) taken on a DRON-4-07 diffractometer (Cu Kα radiation; 40 kV, 18 mA). Data were collected in the range $2\theta = 10 - 150°$ in step mode with the step $\Delta 2\theta = 0.02°$ and an exposure time of 6 s each point. SiO_2 (2θ standard) and NIST SRM1976-Al_2O_3 (certified intensity standard) were used as external standards [4]. The crystal parameters were refined using Rietveld full-profile analysis (FullProf program, version 3.5d).

The electrical properties were measured on a PGSTAT-30 impedance analyzer (Solartron) in a frequency range of 10 Hz – 1 MHz. Silver applied to samples by thermohemical method was used as electrodes. Samples ca. 9 mm in diameter and ca. 3 mm in thickness were used for measurements. The equivalent circuit was determined using the computer program Frequency Response Analyzer 4.7.

3. Results and Discussion

Figures 2 and 3 show fragments of diffractograms for the systems **I** and **II** with different amounts of Li (x). XRPD in the range x = 0 – 0.25 indicates the formation of synthesis single-phase products with defect-perovskite structure of orthorhombic symmetry (space group Pmmm) for the first system and tetragonal symmetry (space group P4/mmm) for the second system. At x > 0.25, when the relation $[Li^+]/[\square] > 1$ (where $[Li^+]$ and $[\square]$ are the number of lithium ions and vacancies, respectively) holds, a lithium metaniobate ($LiNbO_3$) and lithium metatantalate ($LiTaO_3$) with pseudoilmenite structure (space group R3c) are present in addition to the phase with perovskite structure for systems **I** and **II** respectively. The amount of these phases increases with x, and they are predominant at x ≈ 0.47. It should be noted that the phase composition has a poor reproducibility in the single-phase region established (x = 0-

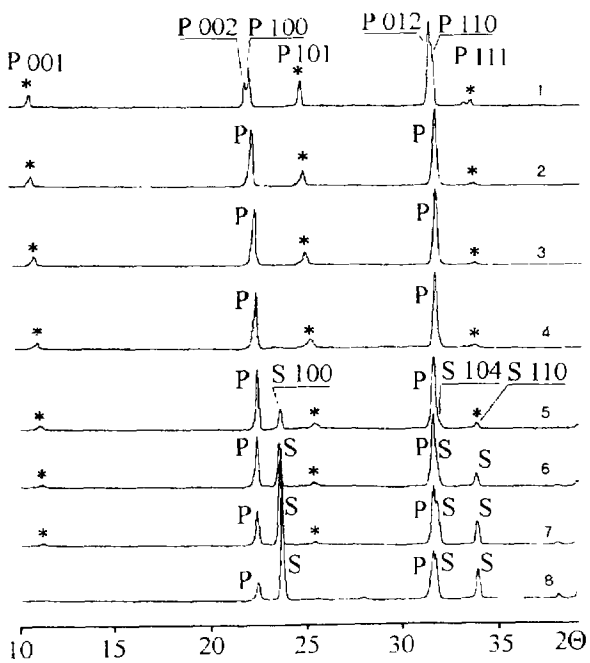

Fig. 2. XRPD for $La_{2/3-x}Li_{3x}\square_{4/3-2x}Nb_2O_6$ samples at various x: 0 (1), 0.166 (2), 0.206 (3), 0.246 (4), 0.286 (5), 0.366 (6), 0.466 (7), 0.516 (8); P = defect perovskite; S = second phase $LiNbO_3$; * indicate superstructure reflections.

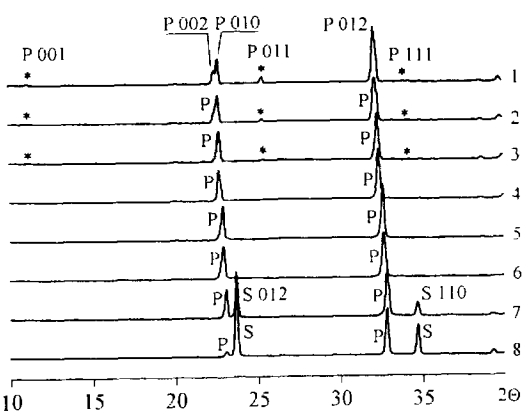

Fig. 3. XRPD for $La_{2/3-x}Li_{3x}\square_{4/3-2x}Ta_2O_6$ samples at various x: 0 (1), 0.126 (2), 0.166 (3), 0.206 (4), 0.246 (5), 0.286 (6), 0.406 (7), 0.616 (8); P = defect perovskite; S = second phase $LiTaO_3$; * indicate superstructure reflections.

Table 1. Structure parameters of complex oxides in the system $La_{2/3-x}Li_{3x}Nb_2O_6$ as a function of lithium content (x).

Composition	$La_{0.64}Li_{0.08}Nb_2O_6$	$La_{0.56}Li_{0.32}Nb_2O_6$	$La_{0.5}Li_{0.5}Nb_2O_6$	$La_{0.46}Li_{0.62}Nb_2O_6$	$La_{0.42}Li_{0.74}Nb_2O_6$
Unit cell parameters					
a (Å)	3.9184(1)	3.906(2)	3.9002(1)	3.8948(1)	3.8943(1)
b (Å)	3.9086(1)	3.907(2)	3.9005(2)	3.9112(2)	3.900(1)
c (Å)	7.9081(2)	7.8785(2)	7.8521(2)	7.7936(5)	7.794(2)
V (Å^3)	121.115(6)	120.21(9)	119.452(6)	118.72(1)	118.38(5)
Positions of atoms (z/c)					
Nb	0.2610(2)	0.2596(2)	0.2580(2)	0.2545(4)	0.2503(7)
$O_3[O_4]$	0.234(1)	0.233(1)	0.232(1)	0.220(3)	0.208(4)
Agreement factors					
Rb (%)	7.14	8.39	9.14	9.57	15.1
Rf (%)	6.69	6.76	6.98	8.30	13.3
Interatomic spacing Nb–O, Å					
Nb–O_1	2.064 (5)	2.045 (5)	2.026 (5)	1.98 (2)	1.95 (2)
Nb–O_2	1.890(4)	1.894 (4)	1.900 (4)	1.91 (1)	1.94 (1)
Nb–O_3, x2	1.966 (3)	1.965 (5)	1.961 (3)	1.97 (1)	1.98 (2)
Nb–O_4, x2	1.971 (3)	1.964 (5)	1.961 (3)	1.96 (1)	1.98 (2)
⟨Nb–O⟩	1.971(4)	1.966(5)	1.962(4)	1.963(1)	1.967(2)
Bottleneck size, S, Å^2					
1(a) ↔ 1(a)[1]	14.48	14.31	14.17	13.25	12.42
1(a) ↔ 1(c)[2]	15.32	15.26	15.21	15.23	15.19
1(c) ↔ 1(c)[3]	16.44	16.39	16.37	16.89	17.51

[1] $|O_1–O_1| \cdot |O_4–O_4| \cdot \sin\alpha_2$, [2] $|O_3–O_3| \cdot |O_4–O_4| \cdot \sin\alpha_3$, [3] $|O_2–O_2| \cdot |O_3–O_3| \cdot \sin\alpha_1$; $|O_2–O_2| = a$.

Table 2. Structure parameters of complex oxides in the system $La_{2/3-x}Li_{3x}Ta_2O_6$ as a function of lithium content (x).

Composition	$La_{0.66}Ta_2O_6$	$La_{0.54}Li_{0.38}Ta_2O_6$	$La_{0.5}Li_{0.5}Ta_2O_6$	$La_{0.46}Li_{0.62}Ta_2O_6$	$La_{0.42}Li_{0.74}Ta_2O_6$
Unit cell parameters					
a (Å)	3.91692(5)	3.9108(1)	3.9030(2)	3.8927(9)	3.8739(2)
c (Å)	7.9109(1)	7.8836(3)	7.8307(7)	7.782(3)	7.7656(7)
V (Å^3)	121.371(3)	120.575(7)	119.29(1)	117.92(7)	116.54(1)
Positions of atoms (z/c)					
Ta	0.2598(2)	0.2591(2)	0.2527(6)	0.2498(5)	0.2495(6)
O_3	0.232(2)	0.231(2)	0.208(5)	0.213(5)	0.227(5)
Agreement factors					
Rb (%)	5.76	8.67	7.06	7.81	8.4
Rf (%)	5.90	7.36	7.03	6.46	7.79
Interatomic spacing Ta–O, Å					
Ta–O_1	2.055(5)	2.043(5)	1.98(1)	1.94(1)	1.94(1)
Ta–O_2	1.900(4)	1.899(4)	1.94(1)	1.947(9)	1.95(1)
Ta–O_3, x4	1.971(5)	1.968(7)	1.98(2)	1.97(2)	1.95(1)
⟨Ta–O⟩	1.973(5)	1.969(5)	1.97(2)	1.96(1)	1.95(1)
Bottleneck size, S, Å^2					
1(a) ↔ 1(a)[1]	14.35	14.21	12.51	12.74	13.60
1(a) ↔ 1(c)[2]	15.34	15.30	15.23	15.16	15.01
1(c) ↔ 1(c)[3]	16.56	16.53	17.63	17.23	16.36

[1] $|O_2–O_2| \cdot |O_3–O_3| \cdot \sin\alpha_1$; $|O_2–O_2| = a$, [2] $|O_1–O_1| \cdot |O_3–O_3| \cdot \sin\alpha_2$; $|O_1–O_1| = a$, [3] $|O_3–O_3|^2$; $|O_3–O_3| = a$; $\alpha_3 = 90^0$.

0.25) for both systems under investigation. For the system **I** the presence of $LiNbO_3$ (1-5 wt.%) and for the system **II** the presence of $LaTaO_{14}$ (2-5 wt.%) may be observed in addition to the perovskite phase. This may be associated with a loss of lithium on heat treatment, which is 15-30 wt.% for the system **I** and 10-20 wt.% for the system **II**. The presence of superstructure reflections in diffractograms for the basic compounds **III** and **IV** (marked with asteriks) indicates ordering of lattice vacancies [7,8], and their broadening and the decrease in their intensity with increasing amount of lithium (x) indicate statistical occupation of vacent sites and a decrease in the degree of order.

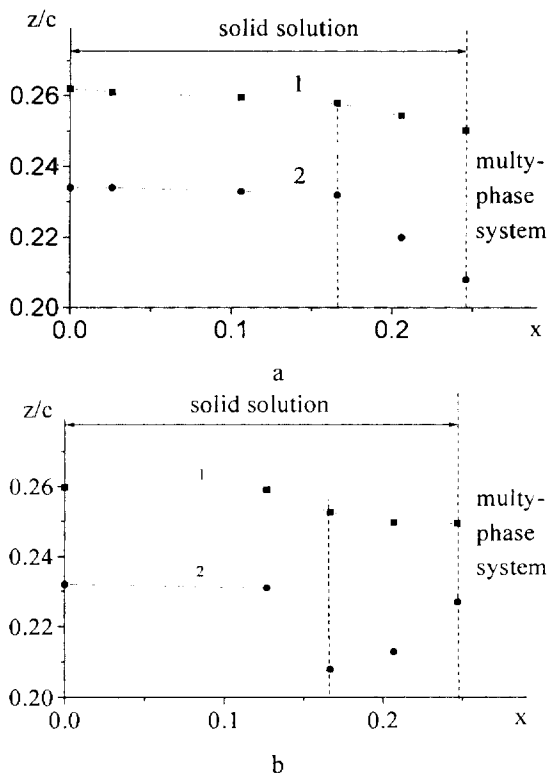

Fig. 4. Positions of Nb[Ta] (1) and $O_3[O_4]$ (2) atoms along the Z axis as a function of lithium content (x) in the system $La_{2/3-x}Li_{3x}\square_{4/3-2x}Nb_2O_6$ (a) and $La_{2/3-x}Li_{3x}\square_{4/3-2x}Ta_2O_6$ (b)

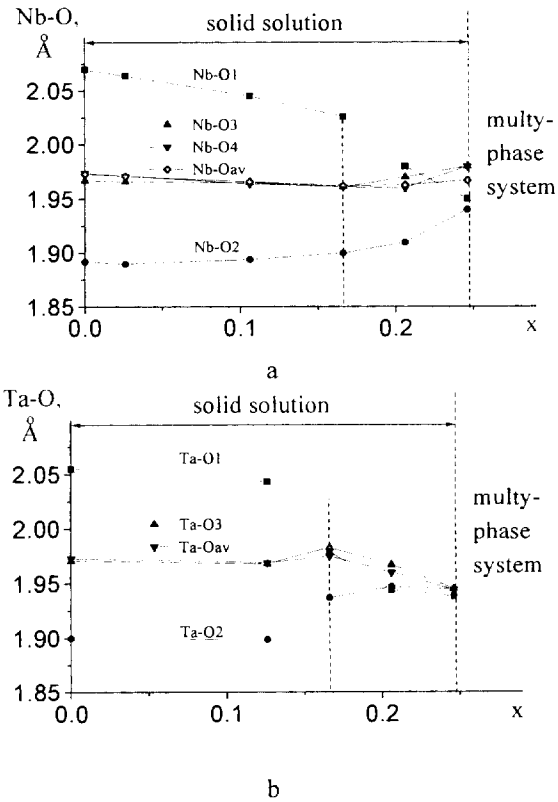

Fig. 5. Nb[Ta]–O interatomic distances in the $Nb[Ta]O_6$ octahedron as a function of lithium content (x) in the system $La_{2/3-x}Li_{3x}\square_{4/3-2x}Nb_2O_6$ (a) and $La_{2/3-x}Li_{3x}\square_{4/3-2x}Ta_2O_6$ (b)

The superstructure reflections disappear for systems **I** and **II** at x = 0.29 and 0.21, respectively. In this case, the symmetry of distorted perovskites increases to cubic one.

Structure parameters of samples **I** and **II** as a function of lithium content are given in the Tables 1 and 2, respectively. The coordinates of the corresponding atoms in the structures **III** [2] and **IV** [5] were taken as the reference atomic coordinates. As follows from Tables 1 and 2, substitution of lithium for lanthanum in samples **I** and **II** shifts the coordinates of niobium (tantalum) atoms and the oxygen atoms lying on the unit cell faces along the *Z* axis. An analysis of the variation of the Nb–O and Ta–O interatomic distances in the oxygen octahedra of the structures **I** and **II** as a function of the amount of lithium (x) is illustrated in Fig. 4. The displacement of Nb [Ta] atoms along the *Z* axis towards the "empty" cuboctahedra (1c) in the basic structures **III** and **IV** is caused by the unsymmetrical electrostatic interaction (repulsion) between Nb [Ta] atoms and the positive charge of the second coordination sphere (in Fig. 1, the site 1a is occupied by 2/3 La + 1/3 ❑ and the site 1c by ❑). It is obvious that when the "empty" layer (1c sites) is filled with cations, Nb [Ta] atoms will be displaced in the direction of the 1a plane. This is observed in the lithium-containing structures **I** and **II** (Tables 1 and 2, Fig. 3). As follows from Fig. 5 the Nb[Ta]–O_2 interatomic distance decreases with increasing amount of lithium (x). Nb [Ta] atoms are displaced towards 1a sites (Fig. 1) and reach symmetrical arrangement along the *Z* axis: Nb-O_1 = Nb–O_2 in samples **I** at x ≈ 0.25 and Ta–O_1 = Ta–O_2 in samples **II** at x ≈ 0.21. The kink in plots of the Nb–O and Ta–O interatomic distances against lithium concentration allows us to assume preferential occupation of 1a sites by Li^+ cations in the range x = 0 – 0.17 for **I** and x = 0 – 0.13 for **II**, and 1c sites at *x* exceeding the above values. The observed difference in the concentration dependences of the Nb–O and Ta–O interatomic distances may be due to the difference in the real lithium content of samples **I** and **II**.

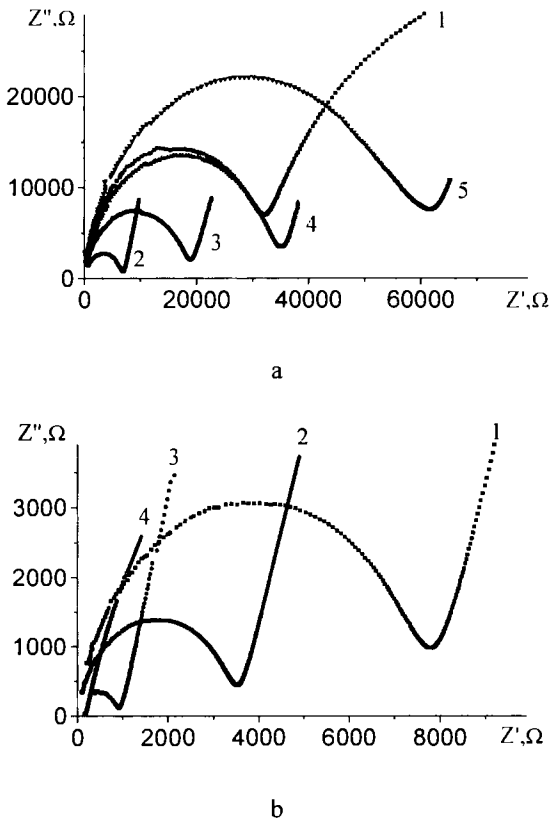

Fig. 6. Complex impedance spectra of the system $La_{2/3-x}Li_{3x}\square_{4/3-2x}Nb_2O_6$, a) at various x: 0.026(1); 0.106(2); 0.166(3); 0.206(4); 0.246(5); T = 290 K, b) at various temperatures: 290 K (1); 315 K (2); 340 K (3); 390 K (4); x = 0.166.

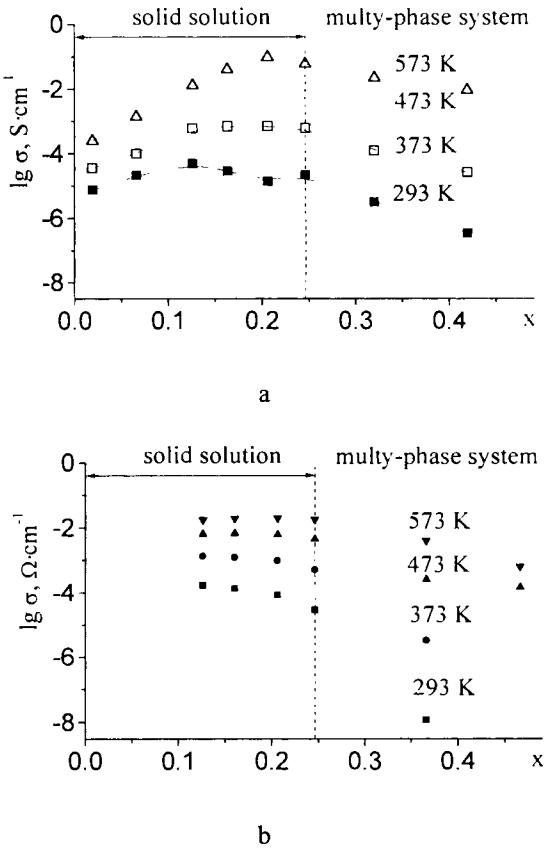

Fig. 7. Isoterms for electrical conductivity against the amount of lithium (x) in the system $La_{2/3-x}Li_{3x}\square_{4/3-2x}Nb_2O_6$ (a) and $La_{2/3-x}Li_{3x}\square_{4/3-2x}Ta_2O_6$ (b).

Figure 6 shows complex impedance plots at various lithium content and at various temperature for samples of the system **I** (for system **II** the complex impedance plots are similar, therefore it is inexpedient to give it in the paper). On the basis of the results of complex impedance, concentration dependences of the electrical conductivity (T = 293 – 573 K) and activation energy of samples **I** and **II** have been calculated, which are shown in Figs. 7 and 8, respectively. The increase in room-temperature conductivity to $\sigma \approx 10^{-4}$ S·cm^{-1} for samples **I** and to $\sigma \approx 5 \cdot 10^{-4}$ S·cm^{-1} for samples **II** with increasing x (Fig. 7, x = 0.13) is caused by an increase in charge carrier concentration at a fairly large number of unoccupied vacancies ([□] = 1.08). The decrease in conductivity and increase in activation energy in the range x = 0.13 – 0.25 (Fig. 8) are accounted for by a decrease in the number of vacant sites ([□] = 0.84 at x = 0.25) and narrowing of migration channel (Table 1 and 2), and at x > 0.25 also by the contribution of the lithium-conducting phase $LiNbO_3$ and $LiTaO_3$ for samples **I** and **II**, respectively, with lower conductivity ($\sigma \approx 10^{-6}$ S·cm^{-1} for **I** and $\sigma \approx 5 \cdot 10^{-6}$ S·cm^{-1} for **II** at 293 K [9]). With rising temperature, the conductivity of samples **I** reaches the following value: $\sigma \approx 10^{-3}$ S·cm^{-1} at 373 K, $\sigma \approx 10^{-1}$ S·cm^{-1} at 573 K, and that of samples **II**: $\sigma \approx 10^{-3}$ S·cm^{-1} at 373 K, $\sigma \approx 0.5 \cdot 10^{-1}$ S·cm^{-1} at 573 K.

The activation energy of conductivity of samples **I** and **II** in the single-phase region is 0.32 – 0.48 eV and 0.28 – 0.37 eV, respectively. This corresponds E_a of solid electrolytes with lithium ion conduction.

The electrical conductivity of a material is known to determined by the concentration and mobility of charge carriers. One of the important factors that determine the ion mobility is the size of migration channels. Tables 1 and 2 list sizes of the so-called "bottleneck", S, [10] between the

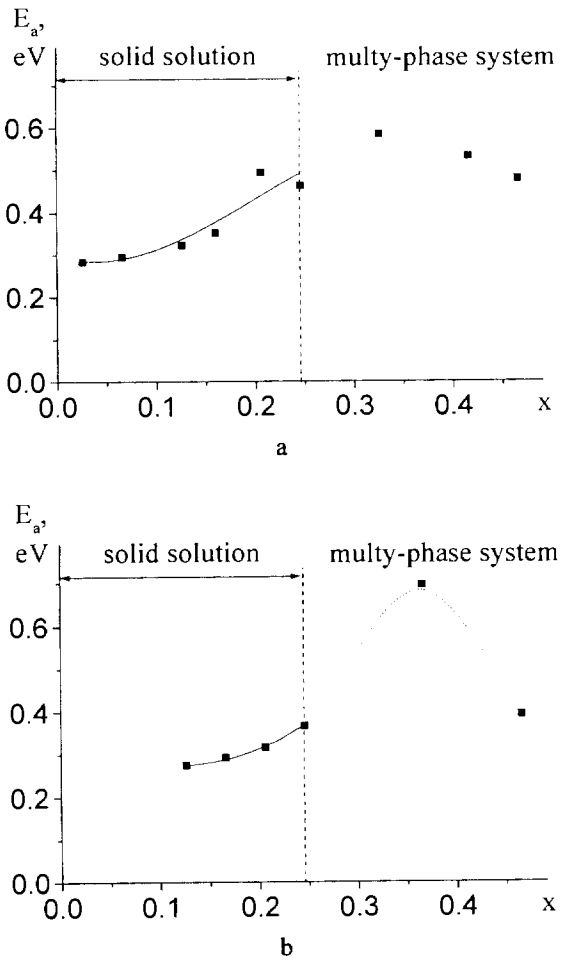

Fig. 8. Activation energy of conductivity (E_a) for $La_{2/3-x}Li_{3x}\square_{4/3-2x}Nb_2O_6$ samples as a function of lithium content (x).

sites 1a↔1a, 1a↔1c and 1c↔1c for lithium ion transport, which were calculated as the area of a parallelogram, in the middles of whose sides oxygen ions are located. As x increases the S value between sites 1a↔1c does not practically change, and between sites 1a↔1a and 1c↔1c it varies symbately to the concentration dependence of the Nb[Ta]–O_1 and Nb[Ta]–O_2 interatomic distances (Tables 1 and 2, Fig. 5). The mobility of cations is known to be determined by the optimum ratio of their size to that of migration channels [1]. Reference [11], which deals with the study of the relation of lithium ion mobility to the size of migration channels, shown that the ion transport in lithium-containing lanthanum titanate with defect-perovskite structure can take place at an interatomic distance of not under 3.96 Å (Li–O = 1.99 Å). Taking into account the said above and the correlation between the concentration dependences of electrical conductivity (Fig. 7), activation energy (Fig. 8), and the "bottleneck" size in the direction 1c↔1c (Tables 1 and 2), it may be concluded that this direction is energetically a favourable pathway of lithium ion migration in complex oxides **I** and **II**.

4. Conclusion

The homogeneity range of solid solutions $La_{2/3-x}Li_{3x}\square_{4/3-2x}Nb_2O_6$ and $La_{2/3-x}Li_{3x}\square_{4/3-2x}Ta_2O_6$ with defect-perovskite structure at x = 0 – 0.25 has been determined, and structure parameters have been refined. It has been found that when Li^+ is substituted for La^{3+} in the structure of $La_{2/3}\square_{4/3}Nb_2O_6$ and $La_{2/3}\square_{4/3}Ta_2O_6$, Nb[Ta] atoms are displaced along the *Z* axis towards the layer of occupied cuboctahedra (site 1a) and reach symmetrical arrangement at x = 0.25 and x = 0.21, respectively.

It has been shown that in the structure of $La_{2/3-x}Li_{3x}\square_{4/3-2x}Nb_2O_6$ and $La_{2/3-x}Li_{3x}\square_{4/3-2x}Ta_2O_6$, Li^+ cations can occupy preferably 1a sites in the range x = 0 – ≈ 0.17 and x = 0 – 0.13, respectively, and 1c sites at x exceeding the above values.

Transport properties of the solid solutions $La_{2/3-x}Li_{3x}\square_{4/3-2x}Nb_2O_6$ and $La_{2/3-x}Li_{3x}\square_{4/3-2x}Ta_2O_6$ have been studied. It was noted that the direction 1c↔1c is energetically a more favorable pathway of lithium ion migration.

It has been shown that materials with high lithium ion conductivity ($\sigma \approx 10^{-1}$ S·cm^{-1} at 573 K) can be produced on the basis of lithium-containing lanthanum metaniobates and metatantalates.

5. References

[1] P.N. Yyer and A.I. Smith, Acta crystallogr. **23**, 740 (1967).

[2] V.K. Trunov, A.A. Yevdokimov, A.M. Frolov and I.M. Averina, Kristallografiya **26**, 189 (1981).

[3] G. Blasse and A. Briel, Z. Phys. Chem. Neue. Folge **57**, 187 (1968).

[4] O.G. Dyachenko, S.Y. Istomin, A.M. Abakumov and E.V. Antipov, Inorgan. Mater. **36**, 315 (2000).

[5] V.K. Trunov, L.N. Lykova and I.S. Afonsky, Vestnik of the Moscow University **1**, 55 (1968).

[6] Certificate of Analysis, Standard Reference Material 1976. National Institute of Standards & Technology, Gaithersburg, 1991, p. 1.

[7] Y. Torii, T. Schiye and T. Yamamato, Mater. Res. Bull. **17**, 727 (1982).

[8] V.B. Nalbandyan and I.A. Shukaev, Zhurn. Neorg. Khim. **34**, 793 (1989).

[9] A.M. Glass, K. Nassau and T.J. Negran, J. Appl. Phys. **49**, 4808 (1978).

[10] L. Latie, G. Villeneuve, D. Conte and G. Le Flem, J. Sol. State Chem. **51**, 293 (1984).

[11] M.A. Paris, J. Sanz, C. Leon, J. Ibarra and A. Varez, Chem. Mater. **12**, 1694 (2000).

Paper presented at the 9th EuroConference on Ionics, Ixia, Rhodes, Greece, Sept. 15 – 21, 2002.

Manuscript rec. Sept. 15, 2002; acc. Jan. 7, 2003.